JACS
JOURNAL OF THE AMERICAN CHEMICAL SOCIETY
Communication
pubs.acs.org/JACS

Formation of Fe_2O_3 Microboxes with Hierarchical Shell Structures from Metal–Organic Frameworks and Their Lithium Storage Properties

Lei Zhang,[†] Hao Bin Wu,[†,‡] Srinivasan Madhavi,[‡] Huey Hoon Hng,[‡] and Xiong Wen (David) Lou*[,†]

[†]School of Chemical and Biomedical Engineering, Nanyang Technological University, 70 Nanyang Drive, Singapore 637457, Singapore

[‡]School of Materials Science and Engineering, Nanyang Technological University, 50 Nanyang Avenue, Singapore 639798, Singapore

Supporting Information

ABSTRACT: Fe_2O_3 microboxes with hierarchically structured shells have been synthesized simply by annealing Prussian blue (PB) microcubes. By utilizing simultaneous oxidative decomposition of PB microcubes and crystal growth of iron oxide shells, we have demonstrated a scalable synthesis of anisotropic hollow structures with various shell architectures. When evaluated as an anode material for lithium ion batteries, the Fe_2O_3 microboxes with a well-defined hollow structure and hierarchical shell manifested high specific capacity (~950 mA h g^{-1} at 200 mA g^{-1}) and excellent cycling performance.

Hollow micro/nanostructures with controllable size, shape, composition, and shell/internal structure have received great attention because of their numerous promising applications in a wide range of fields, such as energy storage and conversion, catalysis, gas sensing, and biomedicine.[1−6] Anisotropic hollow structures with nonspherical shapes and complex hierarchical architectures are particularly interesting for some applications.[7,8] Conventional templating methods to create nonspherical hollow structures still suffer from many difficulties, ranging from forming uniform coatings around high-curvature surfaces to the paucity of nonspherical templates available.[7,8] Recently, several novel approaches based on different principles such as the Kirkendall effect,[9,10] galvanic replacement,[11,12] chemical etching,[13−15] solid-state decomposition,[16] a quasi-templating process,[17] and self-organization of crystallites[18,19] have been developed to prepare anisotropic hollow structures with a variety of compositions, including noble metals and transition-metal oxides/sulfides. One particularly appealing approach for fabricating metal oxide hollow structures on a large scale is by solid-state decomposition and/or conversion of proper solid precursors. Nevertheless, most of the precursors are still limited to unstable metal salts/hydroxides.[16,20] Notwithstanding these advances, the rational design and controllable synthesis of high-quality anisotropic hollow structures with complex hierarchical architectures still remain as significant challenges.

Metal–organic frameworks (MOFs) created from supramolecular assembly of inorganic components (metal ions or metal clusters) with organic components (organic or organometallic complexes) can exhibit diverse architectures and morphologies, such as cubic/octahedral particles, arrow-/platelike particles, hexagonal lumps, and one-dimensional rods/fibers/tubes.[21−31] Therefore, the formation of hollow structures using MOFs as precursors/templates may provide a unique opportunity to develop a new class of highly tailorable functional nanomaterials. For example, MOFs microspheres have been used as sacrificial templates to prepare several hollow and multi-ball-in-ball hybrid metal oxides by taking advantage of the unique reactivity and thermal behavior of MOFs.[28,29] Lin and co-workers synthesized hollow silica rods with various thicknesses and aspect ratios using nanoscale MOFs templates.[32] Chen and co-workers reported the fabrication of hollow ZnS polyhedra based on the reaction of nanoscale ZIF-8 as the sacrificial template and thioacetamide as the sulfur precursor.[25] Despite the progress achieved to date, research on the facile synthesis of nanostructured inorganic functional materials derived from MOFs is still in its very early stage. It is hence highly desirable to develop novel synthesis protocols and concepts utilizing the chemical properties of MOFs to prepare high-quality functional nanomaterials with unique architectures.

Herein we report a scalable synthesis of Fe_2O_3 microboxes with various shell structures based on simple annealing of preformed Prussian blue (PB) microcubes. PB is considered as the first example of a synthetic coordination compounds (or MOFs) consisting of a mixed-valence iron(III) hexacyanoferrate(II) compound of composition $Fe_4[Fe(CN)_6]_3$ with a face-centered-cubic (fcc) crystal structure.[33−36] By taking advantage of the unique reactivity and thermal behavior of PB microcubes, we formed Fe_2O_3 microboxes by an annealing treatment and studied the evolution of the shell structure. When evaluated as an anode material for lithium ion batteries (LIBs), the as-synthesized Fe_2O_3 microboxes manifested high specific capacity and excellent cycling performance.

The strategy for synthesizing Fe_2O_3 microboxes with various shell structures is schematically depicted in Figure 1. First, an improved method for the synthesis of highly uniform PB microcubes was developed. The subsequent thermal transformation process to convert PB microcubes into Fe_2O_3 microboxes can be generally divided into three stages. In stage I, which occurs below 350 °C, a large temperature gradient existing along the radial direction leads to the

Received: July 30, 2012
Published: October 11, 2012

dx.doi.org/10.1021/ja307475c | J. Am. Chem. Soc. 2012, 134, 17388−17391

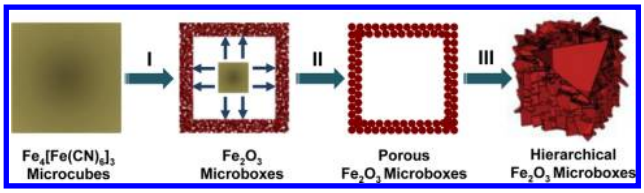

Figure 1. Schematic illustration of the formation of hollow Fe_2O_3 microboxes and the evolution of the shell structure with the increasing calcination temperature.

transformation of PB into iron oxide in the near-surface region.[37] During the thermally induced oxidative decomposition, the continuous decomposition of the PB microcubes is accompanied by outward gas flow, which eventually results in the formation of a relatively dense iron oxide shell and a large interior cavity. With an increase in the annealing temperature to 550 °C (stage II), the Fe_2O_3 microboxes with a relatively smooth and dense shell are transformed into highly porous microboxes constructed from enlarged Fe_2O_3 nanoparticles as a result of crystal growth. Interestingly, further increasing the annealing temperature to 650 °C (stage III) causes the transformation of the highly porous shell into a well-defined hierarchically structured shell consisting of Fe_2O_3 nanoplatelets. The detailed morphological and structural characterizations will be discussed shortly. Compared with the widely used solution-based methods for creating anisotropic hollow structures, the present solid-state approach provides a more facile route for large-scale synthesis of uniform anisotropic hollow structures.

PB microcubes prepared via a facile solution method [see the Experimental Section in the Supporting Information (SI)] were used as the starting material. Panoramic field-emission scanning electron microscopy (FESEM) images showed that these PB microcubes were highly uniform with an average size of ca. 1 μm (Figure 2a and Figure S1 in the SI). A magnified FESEM image (Figure 2b) revealed the very smooth surface over the whole particle, suggesting the single-crystal-like character of the PB microcubes. The crystalline structure of the PB microcubes

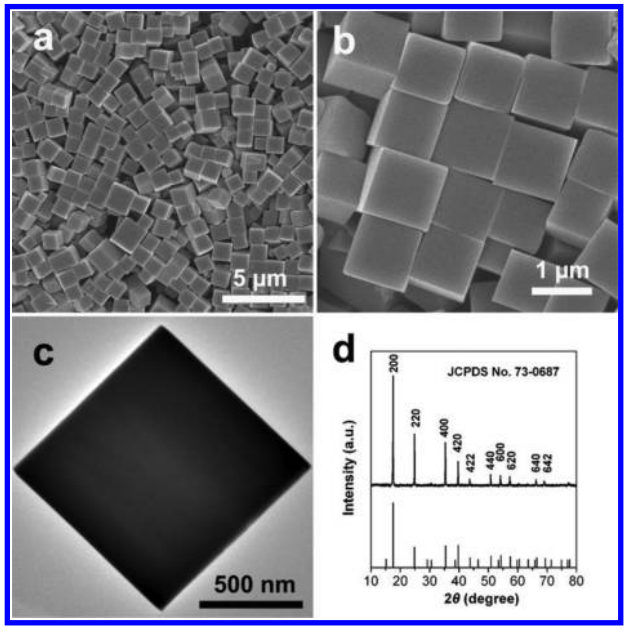

Figure 2. (a, b) FESEM and (c) TEM images and (d) XRD pattern of PB microcubes.

was further characterized by selected-area electron diffraction (SAED) (Figure S2). The SAED pattern can be indexed to the [001] zone axis of cubic PB microcubes. This observation evidently suggests the single-crystalline characteristic of the PB microcubes. A uniform-contrast transmission electron microscopy (TEM) image of a single microcube clearly demonstrated its solid and dense nature without discernible porosity (Figure 2c). The crystallographic structure and phase purity of the PB microcubes were examined by powder X-ray diffraction (XRD). As can be seen from the XRD pattern in Figure 2d, all of the diffraction peaks could be unambiguously assigned to fcc $Fe_4[Fe(CN)_6]_3$ (JCPDS card no. 73-0687; space group $Fm3m$, $a = b = c = 10.13$ Å, $\alpha = \beta = \gamma = 90°$). No additional diffraction peaks from impurities were detected, indicating the high purity of the product.

The as-prepared PB microcubes were transformed into Fe_2O_3 microboxes by annealing in air. As indicated by thermogravimetric analysis (TGA) (Figure S3), the PB microcubes underwent significant weight loss mainly below 320 °C, during which PB decomposed into iron oxide. The thermal transformation process was performed at three temperatures: 350, 550, and 650 °C. The Fe_2O_3 microboxes obtained at different temperatures with distinct morphologies and structures are displayed in Figure 3. At a relatively low

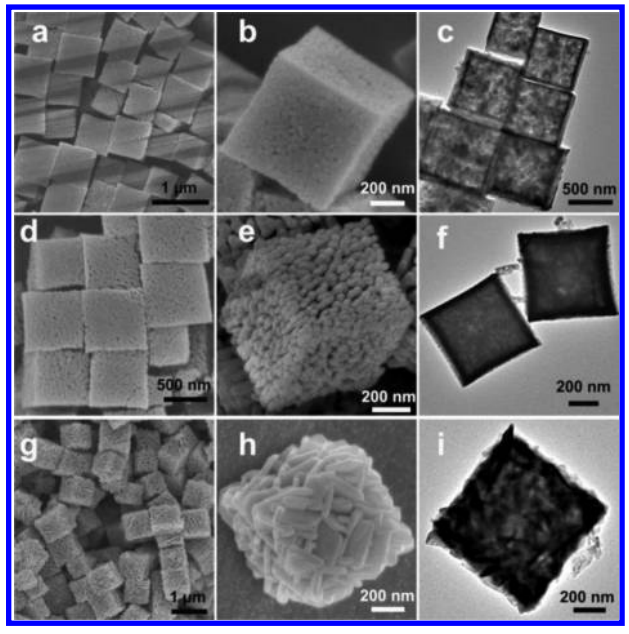

Figure 3. (a, b, d, e, g, h) FESEM and (c, f, i) TEM images of hollow Fe_2O_3 microboxes obtained at (a, b, c) 350 °C, (d, e, f) 550 °C, and (g, h, i) 650 °C.

temperature of 350 °C, the Fe_2O_3 microboxes retained well the size and cubic shape of the PB precursor particles (Figure 3a–c). As revealed by the magnified FESEM image (Figure 3b), the surface was relatively smooth, although some small nanopores could still be recognized. XRD analysis (Figure S4) confirmed that the sample was composed of cubic bixbyite β-Fe_2O_3 (JCPDS card no. 39-0238) and cubic spinel γ-Fe_2O_3 (JCPDS card no. 39-1346).[38,39] TEM examination (Figure 3c) clearly showed the existence of a large cavity in each Fe_2O_3 microbox. Hence, during the oxidative decomposition of PB, the iron oxide grew into a relatively smooth and dense crystalline shell, inheriting well the overall cubic morphology of the PB

dx.doi.org/10.1021/ja307475c | J. Am. Chem. Soc. 2012, 134, 17388–17391

microcube.[38,39] More interestingly, such Fe_2O_3 microboxes underwent further crystal growth at increased temperatures. As shown in Figure 3d–f, Fe_2O_3 microboxes with highly porous shells were obtained at 550 °C. The porous microboxes were constructed of Fe_2O_3 nanoparticles with sizes of tens of nanometers, as shown in the magnified FESEM image, while the hollow cubic structure was perfectly retained, as shown in the TEM image. Nonetheless, broken porous microboxes were found after mechanical grinding (Figure S5). After calcination at an elevated temperature of 650 °C, the porous shell of the microboxes further evolved into a complex hierarchical structure consisting of sheetlike Fe_2O_3 subunits (Figure 3g–i and Figure S6). It is worth noting that even after the annealing at 650 °C, the cubic hollow structure still remained intact with almost no broken microboxes observed, suggesting the excellent structural stability of the Fe_2O_3 microboxes. XRD analysis (Figure S4) revealed that the diffraction peaks of both β-Fe_2O_3 and γ-Fe_2O_3 became more intense and sharper in the Fe_2O_3 microboxes obtained at 550 and 650 °C, again providing evidence of the growth of Fe_2O_3 crystallites and the structural evolution at elevated temperatures. Therefore, the whole thermal transformation process is characterized by two major phases: thermally induced oxidative decomposition of the PB microcubes and further crystal growth of Fe_2O_3. The former creates the hollow structure of the Fe_2O_3 microcubes, while the later leads to the formation of different shell architectures. The texture and porosity of the samples were also characterized by measuring N_2 adsorption–desorption isotherms (Figure S7). The Fe_2O_3 microboxes obtained at 350 °C showed a moderate Brunauer–Emmett–Teller (BET) specific surface area of 52.2 $m^2\ g^{-1}$, which is much higher than that of the pristine dense PB microcubes (3.7 $m^2\ g^{-1}$). As expected, the interesting evolution of the shell architecture at elevated temperatures was accompanied by a considerable decrease in the BET specific surface area to 37.4 $m^2\ g^{-1}$ for the porous Fe_2O_3 microboxes obtained at 550 °C and finally to 25.4 $m^2\ g^{-1}$ for the hierarchical Fe_2O_3 microboxes obtained at 650 °C.

As an important member of the transition-metal oxide family, Fe_2O_3 has long been regarded as a very promising anode material for LIBs because of its much higher theoretical capacity of ~1000 mA h g^{-1} compared with that of conventional graphite-based anodes (372 mA h g^{-1}) as well as their nontoxicity, high corrosion resistance, and low processing cost.[40,41] Despite the relatively high charge/charge potential that reduces the voltage in full cells, the improved safety, high capacity, and low cost still make Fe_2O_3 an attractive anode material. Also, the drawback of relatively low Coulombic efficiency in the initial cycle could be partly overcome by a prelithiation treatment. In view of their unique nanostructures and excellent stability, these Fe_2O_3 microboxes might serve as promising anode materials for future LIBs. Hence, electrochemical measurements were carried out to evaluate the performance of Fe_2O_3 microboxes with different shell structures. The discharge–charge voltage profiles of a representative sample (porous Fe_2O_3 microboxes obtained at 550 °C) are shown in Figure 4a. A distinct voltage plateau at ca. 0.75 V was clearly identified during the initial discharge process, and it shifted to ca. 1.0 V and remained stable in the subsequent cycles. Meanwhile, a poorly defined plateau was observed in the charge process at ca. 1.8 V. The discharge–charge voltage profiles are in good agreement with previous reports, which correspond to the reversible reduction of Fe_2O_3 to Fe^0 and the simultaneous formation of Li_2O based on the following

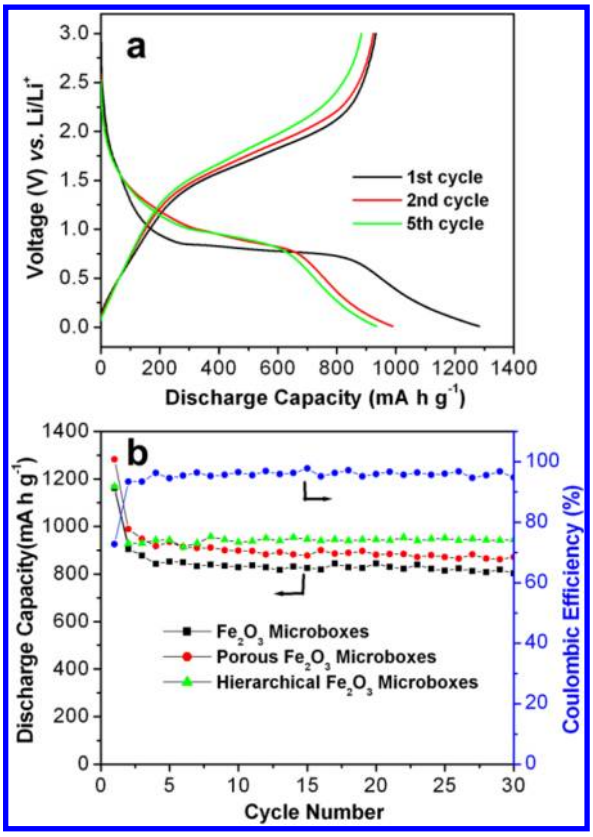

Figure 4. (a) Discharge–charge voltage profiles of porous Fe_2O_3 microboxes obtained at 550 °C. (b) Cycling performance of Fe_2O_3 microboxes (350 °C), porous Fe_2O_3 microboxes (550 °C), and hierarchical Fe_2O_3 microboxes (650 °C) and Coulombic efficiency of porous Fe_2O_3 microboxes (550 °C) over the voltage range 0.01–3.0 V vs Li/Li^+ at the same current density of 200 mA g^{-1}.

conversion half-reaction: $Fe_2O_3 + 6Li^+ + 6e^- \rightleftarrows 2Fe^0 + 3Li_2O$.[40,41] To evaluate the cycling stability, the three samples (Fe_2O_3 microboxes, porous Fe_2O_3 microboxes, and hierarchical Fe_2O_3 microboxes) were charged and discharged at a current density of 200 mA g^{-1} over the voltage range 0.01–3.0 V vs Li/Li^+, and the cycling performance is depicted in Figure 4b. Despite the initial capacity loss of ca. 20%, which is considered quite low for transition-metal oxide-based anodes, all three samples displayed excellent cycling stability with almost no fading of capacity over the first 30 cycles. In particular, the hierarchical Fe_2O_3 microboxes obtained at 650 °C exhibited the highest reversible capacity of 945 mA h g^{-1} in the 30th cycle, while comparable capacities of 802 and 871 mA h g^{-1} were also obtained for Fe_2O_3 microboxes (350 °C) and porous Fe_2O_3 microboxes (550 °C), respectively. From the second cycle onward, the Fe_2O_3 microboxes exhibited a Coulombic efficiency of ~95%. The cycling response at continuously varying rates showed that even during cycling at a high current density of 1000 mA g^{-1}, capacities in the range 500–1000 mA h g^{-1} could still be retained (Figure S8). Compared with other reported Fe_2O_3-based materials, the unique hierarchical Fe_2O_3 microboxes manifested greatly enhanced lithium storage properties with high reversible capacity and excellent cyclic capacity retention.[40,41] The remarkable lithium storage properties are probably related to the unique nanostructure of these Fe_2O_3 microboxes. Specifically, both the hollow structure and the porous shell architecture facilitate penetration of the electrolyte and transport of Li^+ ions in the electrode.[40]

dx.doi.org/10.1021/ja307475c | J. Am. Chem. Soc. 2012, 134, 17388–17391

Meanwhile, such hierarchical hollow structures could efficiently buffer the stress caused by volume variation during the charge–discharge process.[13] Furthermore, the Fe_2O_3 microboxes with high crystallinity and structural stability would also help in retaining the pristine nanostructure upon cycling.

In summary, we have demonstrated a facile and scalable synthesis of Fe_2O_3 microboxes with various shell structures. Fe_2O_3 microboxes were formed by thermally induced oxidative decomposition of Prussian blue microcubes at 350 °C. When the annealing temperature was increased to 550 °C, porous Fe_2O_3 microboxes constructed of enlarged Fe_2O_3 nanoparticles were obtained, and hierarchical microboxes constructed of Fe_2O_3 nanoplatelets were produced by annealing at 650 °C. When evaluated as potential anode materials for lithium ion batteries, the as-prepared Fe_2O_3 microboxes with unique shell structures exhibited high lithium storage capacities and excellent cycling performance. By taking advantage of the unique reactivity and thermal behavior of a large number of MOFs synthesized to date with fascinating architectures and morphologies, the present solid-state thermal decomposition method might inspire some new directions for the large-scale synthesis of unique functional nanomaterials. We anticipate that the approach presented in this work could be extended to the fabrication of other hollow structures, compositions, and geometries.

■ ASSOCIATED CONTENT

Supporting Information

Detailed experimental procedures, additional FESEM and high-resolution TEM images, SAED pattern, TGA curve, XRD patterns, N_2 adsorption–desorption isotherms, and rate capability of hierarchical Fe_2O_3 microboxes. This material is available free of charge via the Internet at http://pubs.acs.org.

■ AUTHOR INFORMATION

Corresponding Author

xwlou@ntu.edu.sg

Notes

The authors declare no competing financial interest.

■ ACKNOWLEDGMENTS

We are grateful to the National Research Foundation (Singapore) for financial support through the Clean Energy Research Programme (CERP; NRF2009EWRCERP001-036).

■ REFERENCES

(1) Lou, X. W.; Archer, L. A.; Yang, Z. C. *Adv. Mater.* **2008**, *20*, 3987.
(2) Caruso, F.; Caruso, R. A.; Mohwald, H. *Science* **1998**, *282*, 1111.
(3) Lai, X. Y.; Li, J.; Korgel, B. A.; Dong, Z. H.; Li, Z. M.; Su, F. B.; Du, J. A.; Wang, D. *Angew. Chem., Int. Ed.* **2011**, *50*, 2738.
(4) Liu, J.; Qiao, S. Z.; Hartono, S. B.; Lu, G. Q. *Angew. Chem., Int. Ed.* **2010**, *49*, 4981.
(5) Li, H. X.; Bian, Z. F.; Zhu, J.; Zhang, D. Q.; Li, G. S.; Huo, Y. N.; Li, H.; Lu, Y. F. *J. Am. Chem. Soc.* **2007**, *129*, 8406.
(6) Kim, T.; Momin, E.; Choi, J.; Yuan, K.; Zaidi, H.; Kim, J.; Park, M.; Lee, N.; McMahon, M. T.; Quinones-Hinojosa, A.; Bulte, J. W. M.; Hyeon, T.; Gilad, A. A. *J. Am. Chem. Soc.* **2011**, *133*, 2955.
(7) Hu, M.; Chen, J. Y.; Li, Z. Y.; Au, L.; Hartland, G. V.; Li, X. D.; Marquez, M.; Xia, Y. N. *Chem. Soc. Rev.* **2006**, *35*, 1084.
(8) Shchepelina, O.; Kozlovskaya, V.; Singamaneni, S.; Kharlampieva, E.; Tsukruk, V. V. *J. Mater. Chem.* **2010**, *20*, 6587.
(9) Cao, H. L.; Qian, X. F.; Wang, C.; Ma, X. D.; Yin, J.; Zhu, Z. K. *J. Am. Chem. Soc.* **2005**, *127*, 16024.
(10) Yin, Y. D.; Rioux, R. M.; Erdonmez, C. K.; Hughes, S.; Somorjai, G. A.; Alivisatos, A. P. *Science* **2004**, *304*, 711.
(11) Skrabalak, S. E.; Au, L.; Li, X. D.; Xia, Y. N. *Nat. Protoc.* **2007**, *2*, 2182.
(12) Sun, Y. G.; Mayers, B.; Xia, Y. N. *Adv. Mater.* **2003**, *15*, 641.
(13) Wang, Z. Y.; Luan, D. Y.; Boey, F. Y. C.; Lou, X. W. *J. Am. Chem. Soc.* **2011**, *133*, 4738.
(14) Sui, Y. M.; Fu, W. Y.; Zeng, Y.; Yang, H. B.; Zhang, Y. Y.; Chen, H.; Li, Y. X.; Li, M. H.; Zou, G. T. *Angew. Chem., Int. Ed.* **2010**, *49*, 4282.
(15) An, K.; Kwon, S. G.; Park, M.; Na, H. B.; Baik, S. I.; Yu, J. H.; Kim, D.; Son, J. S.; Kim, Y. W.; Song, I. C.; Moon, W. K.; Park, H. M.; Hyeon, T. *Nano Lett.* **2008**, *8*, 4252.
(16) Wang, L. Z.; Tang, F. Q.; Ozawa, K.; Chen, Z. G.; Mukherj, A.; Zhu, Y. C.; Zou, J.; Cheng, H. M.; Lu, G. Q. *Angew. Chem., Int. Ed.* **2009**, *48*, 7048.
(17) Lou, X. W.; Yuan, C.; Zhang, Q.; Archer, L. A. *Angew. Chem., Int. Ed.* **2006**, *45*, 3825.
(18) Yang, X. F.; Fu, J. X.; Jin, C. J.; Chen, J. A.; Liang, C. L.; Wu, M. M.; Zhou, W. Z. *J. Am. Chem. Soc.* **2010**, *132*, 14279.
(19) He, T.; Chen, D. R.; Jiao, X. L.; Wang, Y. L. *Adv. Mater.* **2006**, *18*, 1078.
(20) Zhou, L.; Zhao, D. Y.; Lou, X. W. *Angew. Chem., Int. Ed.* **2012**, *51*, 239.
(21) Umemura, A.; Diring, S.; Furukawa, S.; Uehara, H.; Tsuruoka, T.; Kitagawa, S. *J. Am. Chem. Soc.* **2011**, *133*, 15506.
(22) Nune, S. K.; Thallapally, P. K.; Dohnalkova, A.; Wang, C. M.; Liu, J.; Exarhos, G. J. *Chem. Commun.* **2010**, *46*, 4878.
(23) Jung, S.; Oh, M. *Angew. Chem., Int. Ed.* **2008**, *47*, 2049.
(24) Jung, S.; Cho, W.; Lee, H. J.; Oh, M. *Angew. Chem., Int. Ed.* **2009**, *48*, 1459.
(25) Jiang, Z.; Sun, H. Y.; Qin, Z. H.; Jiao, X. L.; Chen, D. R. *Chem. Commun.* **2012**, *48*, 3620.
(26) Hui, J. K. H.; MacLachlan, M. J. *Coord. Chem. Rev.* **2010**, *254*, 2363.
(27) deKrafft, K. E.; Wang, C.; Lin, W. B. *Adv. Mater.* **2012**, *24*, 2014.
(28) Cho, W.; Lee, Y. H.; Lee, H. J.; Oh, M. *Adv. Mater.* **2011**, *23*, 1720.
(29) Cho, W.; Lee, Y. H.; Lee, H. J.; Oh, M. *Chem. Commun.* **2009**, 4756.
(30) Cho, W.; Lee, H. J.; Oh, M. *J. Am. Chem. Soc.* **2008**, *130*, 16943.
(31) Hu, L.; Yan, N.; Chen, Q. W.; Zhang, P.; Zhong, H.; Zheng, X. R.; Li, Y.; Hu, X. Y. *Chem.—Eur. J.* **2012**, *18*, 8971.
(32) Rieter, W. J.; Taylor, K. M. L.; Lin, W. B. *J. Am. Chem. Soc.* **2007**, *129*, 9852.
(33) Hu, M.; Furukawa, S.; Ohtani, R.; Sukegawa, H.; Nemoto, Y.; Reboul, J.; Kitagawa, S.; Yamauchi, Y. *Angew. Chem., Int. Ed.* **2012**, *51*, 984.
(34) Vaucher, S.; Li, M.; Mann, S. *Angew. Chem., Int. Ed.* **2000**, *39*, 1793.
(35) Wu, X. L.; Cao, M. H.; Hu, C. W.; He, X. Y. *Cryst. Growth Des.* **2006**, *6*, 26.
(36) Shen, X. P.; Wu, S. K.; Liu, Y.; Wang, K.; Xu, Z.; Liu, W. *J. Colloid Interface Sci.* **2009**, *329*, 188.
(37) Zhong, J. Y.; Cao, C. B.; Liu, Y. Y.; Li, Y. A.; Khan, W. S. *Chem. Commun.* **2010**, *46*, 3869.
(38) Hu, M.; Jiang, J. S.; Zeng, Y. *Chem. Commun.* **2010**, *46*, 1133.
(39) Zboril, R.; Machala, L.; Mashlan, M.; Sharma, V. *Cryst. Growth Des.* **2004**, *4*, 1317.
(40) Wang, B.; Chen, J. S.; Wu, H. B.; Wang, Z. Y.; Lou, X. W. *J. Am. Chem. Soc.* **2011**, *133*, 17146.
(41) Kang, N.; Park, J. H.; Choi, J.; Jin, J.; Chun, J.; Jung, I. G.; Jeong, J.; Park, J. G.; Lee, S. M.; Kim, H. J.; Son, S. U. *Angew. Chem., Int. Ed.* **2012**, *51*, 6626.